



Book review

Testing the applicability of standardised growth curves for chemically heterogeneous single-grain feldspars from the Atacama Desert, Chile

Linda A.E. Maßon^{a,*}, Svenja Riedesel^{a,b}, Anja Zander^a, Mariana Sontag-González^{c,d}, Tony Reimann^a^a Institute of Geography, University of Cologne, Germany^b Luminescence Physics and Technologies, Department of Physics, Technical University of Denmark, Denmark^c Institute of Geography, Justus-Liebig-University Gießen, Germany^d Department of Geosciences, Stony Brook University, NY, 11794-2100, USA

ARTICLE INFO

Keywords:

Feldspar
Single grain pIRIR
Standardised growth curve
Atacama Desert
Single grain geochemistry

ABSTRACT

The Atacama Desert is generally considered the driest non-polar desert on Earth and is therefore an ideal study area for exploring the water and biota free endmember of Earth's Critical Zone (ECZ). Single grain (SG) luminescence dating has successfully identified processes in the ECZ. However, SG luminescence dating of Atacama Desert feldspars is challenging and time consuming since only a small fraction of grains emits sufficient luminescence and their potassium (K) contents, needed for internal dose rate calculations, are highly variable. Here we present an adaption of the standardised growth curve (SGC) method adjusted to the conditions of Atacama Desert sediments and a correlation of single-grain geochemistry and luminescence properties.

To evaluate if SGCs are suitable for our study site and to determine the influence of the K-content on our luminescence age calculations, we used a set of five samples from the Atacama Desert and five chemically and structurally different feldspar sediment extracts from various geological origins worldwide. We performed a dose recovery test (DRT) using a post-infrared infrared stimulated luminescence (pIRIR) protocol and measured nine major element concentrations, including K, on a single grain level using a scanning electron microscope (SEM) with energy-dispersive X-ray spectroscopy (EDX). The DRT dataset was then used to test the application of SGCs. The accuracy of Atacama feldspar pIRIR measurements fitted onto SGCs frequently suffers from odd values in single measurement cycles, since the SGC approach developed for SG feldspar luminescence (Li et al., 2015b) uses one L_x/T_x measurement to project the L_n/T_n values onto a SGC. We investigate the influence of calculating a synthetic regenerative signal (sR) for SGC fitting, to reduce the effect of those odd values on individual grain measurements. Furthermore, we reduced the regenerative cycles used for our sR approach, to test if shorter protocols would result in equivalent dose (D_e) estimates in agreement with longer protocols. We then calculated Spearman rank correlations between the results obtained with our modified SGC and the SAR protocol, luminescence signal intensities, and the geochemical dataset.

Finally, we present a new method of fitting data onto a SGC which significantly decreases measurement time, without risking the inclusion of outliers. We furthermore show that the luminescence signal intensities, the D_e values and their dose recovery ratios obtained with our SGC method and a SAR protocol, are independent of the sample geochemistry.

1. Introduction

In the recent past the interrelationship of life and the evolution of Earth's surface has been subject to intensified research activities (e.g., Amundson et al., 2007; Starke et al., 2020). The outermost shell of our planet, in which rocks, soils, water, air and biota interact and thus where

this interrelationship takes place, is often referred to as the Earth's Critical Zone (ECZ) (Giardino and Houser, 2015). The Atacama Desert in Chile, generally considered the driest non-polar desert on Earth, is an ideal study site to explore the dynamics of the water and biota free endmember of ECZ systems (e.g., Dietrich and Perron, 2006; Oeser et al., 2018; Tchakerian and Pease, 2015). Single-grain luminescence dating

* Corresponding author.

E-mail address: l.masson@uni-koeln.de (L.A.E. Maßon).<https://doi.org/10.1016/j.quageo.2024.101585>

Received 24 October 2023; Received in revised form 23 May 2024; Accepted 23 June 2024

Available online 28 June 2024

1871-1014/© 2024 The Authors. Published by Elsevier B.V. This is an open access article under the CC BY license (<http://creativecommons.org/licenses/by/4.0/>).

has successfully been applied to infer sediment transport and mixing processes in the ECZ in various geological settings dissimilar to the Atacama Desert (Bonnet et al., 2019; Reimann et al., 2017; Román-Sánchez et al., 2019a, 2019b). So far, optically stimulated luminescence (OSL) measurements carried out in the Atacama Desert were merely designed to determine the depositional age of sediments (e.g., Bartz et al., 2020a,b; Del Río et al., 2019; Diederich et al., 2020; May et al., 2015, 2020; Ritter et al., 2019; Veit et al., 2015) and dynamics inside a calcium sulphate wedge (Zinelabedin et al., 2022). Those studies revealed the unfavourable properties of Atacama Desert sediments especially regarding quartz OSL measurements. Quartz from the Atacama Desert has been shown to have a very low OSL sensitivity and unstable signal components (Bartz et al., 2020a; Del Río et al., 2019; May et al., 2015; Veit et al., 2015; Zinelabedin et al., 2022). Furthermore, a previous study on the applicability of luminescence dating of coarse grain feldspars from the Atacama Desert found highly variable potassium (K) contents within each sample and merely ~1 % of the measured feldspar grains gave a post-infrared infrared stimulated luminescence (pIRIR) signal suitable for dating (Zinelabedin et al., 2022). The heterogeneity of K-contents in feldspars poses a challenge in calculating internal dose rates and raises the question of whether the chemical composition of feldspars is related to luminescence properties.

Problematic quartz OSL properties have been reported previously and have been associated with the quartz source area (e.g., Bartz et al., 2020a; Sawakuchi et al., 2011; Tokuyasu et al., 2010), the depositional context of the sample (e.g., Fitzsimmons et al., 2010; Li and Wintle, 1992) or too few reworking cycles (e.g., Sawakuchi et al., 2011; Steffen et al., 2009). In some cases, coping strategies have been developed (Fuchs and Owen, 2008; Sawakuchi et al., 2011). So far, due to its unfavourable OSL properties, quartz has been discarded for luminescence dating of Atacama Desert sediments (e.g. Bartz et al., 2020a; Zinelabedin et al., 2022). Considerably fewer studies have addressed problematic feldspars. Single-grain measurements of feldspars can be challenging and time-consuming, particularly when only a small percentage of grains emits suitable luminescence signals (e.g. Brill et al., 2018; O’Gorman et al., 2021; Sontag-González et al., 2021; Zinelabedin et al., 2022). In such cases many single grain (SG) discs have to be measured before a sufficient number of grains has been obtained to calculate a robust palaeodose. This can result in such samples not being investigated further (Brill et al., 2018). Establishing a standardised growth curve (SGC) for single-grain feldspar pIRIR measurements reduces the measurement time considerably (Li et al., 2018). Sontag-González et al. (2021) showed that SGCs are also suitable for feldspars with unfavourable luminescence properties and a complex mineralogy.

Atacama Desert feldspars studied so far show highly variable K-contents with on average low K-concentrations (Zinelabedin et al., 2022). It is generally considered that a feldspar grain giving a luminescence signal has a K-content in the range of 8–13 % (12.5 ± 0.5 % Huntley and Baril, 1997 or 10 ± 2 % Smedley et al., 2012). Furthermore, Prescott and Fox (1993) (thermoluminescence) and Spooner (1992) (infrared stimulated luminescence) presented data for the whole composition range of the feldspar mineral group, showing a positive

correlation of K-contents and signal intensity. In contrary, O’Gorman et al. (2021) and Zinelabedin et al. (2022) not only showed that grains with lower K-concentrations may emit suitable pIRIR signals but also that the majority of grains in a sample, which are used for D_e calculations, may have K-contents much below the proposed literature values (<3 % and 3.9 ± 1 % respectively). Moreover Smedley et al. (2012) found no correlation between K-content and signal intensity on a single-grain level. In agreement with that Finch and Klein (1999) as well as Riedesel et al. (2021) proposed a different source for signal intensity levels in the blue emission by linking them to Al–O–Al bridges, whereas Garcia-Guinea et al. (1999) connected signal intensity to alkali ion leakages caused by prolonged heating. This raises the question of whether, in the case of Atacama Desert feldspars, single grain K-contents have to be determined for dose rate calculation and if correlations exist between the chemical composition of the feldspars and their luminescence properties.

In this study we aim to establish a methodological framework for time-efficient single-grain luminescence-based analysis of feldspar samples from the Atacama Desert. We use a test dataset consisting of ten samples, five from the Atacama Desert and five chemically and structurally different feldspar sediment extracts from various geological origins from around the world. A dose recovery test (pIRIR₁₇₅) is performed on 500 grains per sample and the geochemistry of 300 out of the 500 grains is determined using a scanning electron microscope (SEM) equipped with an energy-dispersive X-ray spectrometer (EDX). With this dataset we test the applicability of SGCs for single-grain pIRIR equivalent dose (D_e) determination of Atacama Desert feldspars, in order to reduce our measurement times and we use Spearman rank correlations to investigate the influence of geochemistry on luminescence properties and SGC performance.

2. Samples and instrumentation

2.1. Samples

Our sample suite consists of ten samples of different origin and chemical composition. Five samples (ARO-18-08-LP, CSA-1-2-2, LAGU-1-1, PAG-6-4b, PAG-6-6b) originate from the Atacama Desert. The remaining five samples originate from badlands in Canada (ABLR-1), lake sediments in Japan (HAM-5), a beach ridge in Chile ~1000 km south of the Atacama Desert (ISM-7), the Continental Deep Drilling (KTB) borehole in Germany (KTB-383-C) and the Mont-Blanc tunnel in Italy (MBT-I-2430). We chose the non-Atacama samples to reflect a range of chemical and structural variations of feldspar. Basic information on the samples are summarised in Table 1.

Prior to luminescence measurements the samples were sieved and treated with HCl (10 %), H₂O₂ (10 %) and Na₂C₂O₄ (0.01 N), to remove carbonates and organics and to disperse the particles, respectively. Subsequently, samples were sieved again to obtain different grain size fractions (Table 1). A heavy liquid density separation was used to enrich the K-rich feldspar fraction ($\rho < 2.58$ g/cm³). Sample KTB-383-C feldspars were etched with HF afterwards (see Guralnik et al. (2015)

Table 1

Sample description. Sample KTB-383-C was prepared in the laboratory of the University of Lausanne. Sample MBT-I-2430 was prepared at DTU-Risø. All other samples were prepared at the Cologne Luminescence Laboratory.

Sample ID	Origin and subset affiliation	Coordinates		Grain size [μ m]	Grain hole size [μ m]	References
ARO-18-08 LP	Atacama Desert, Chile (A)	19°39'34.02" S	69°35'51.4" W	200–250	300	Zinelabedin et al. (2022)
CSA-1-2-2	Atacama Desert, Chile (A)	19°36'20.17" S	70°5'52.12" W	100–200	250	This study
LAGU-1-1	Atacama Desert, Chile (A)	21°1'59.37" S	69°47'53.00" W	100–250	300	This study
PAG-6-4b	Atacama Desert, Chile (A)	21°32'31.7" S	69°54'47.9" W	100–200	250	Ritter et al. (2019)
PAG-6-6b	Atacama Desert, Chile (A)	21°32'31.7" S	69°54'47.9" W	100–200	250	Ritter et al. (2019)
ABLR-1	Badlands, Canada (X)	50°1'30.6" N	104°59'15.81" W	100–200	250	This study
HAM-5	Lake Hamana, Japan (X)	34°45'8.65" N	137°34'22.62" E	100–200	250	Riedesel et al. (2021), 2019
ISM-7	Beach ridge, Chile (X)	37°1'20.28" S	73°30'43.49" W	100–200	250	This study
KTB-383-C	KTB Borehole, Germany (X)	49°48'55" N	12°7'14" E	180–250	250	Guralnik et al. (2015)
MBT-I-2430	Mount Blanc Tunnel, Italy (X)	45°50'07" N	6°55'59" E	180–212	250	Lambert (2018)

for further details).

2.2. Luminescence

For the dose recovery tests the samples were loaded into standard single-grain discs under a microscope under daylight conditions, for grain hole sizes used see Table 1. A single hair was used to pick the grains ensuring that all 100 holes per disc were filled with one grain each. Despite this, for the samples CSA-1-2-2, HAM-5 and KTB-383-C it was sometimes unavoidable to have several grains in one hole. Prior to the dose recovery test, all mounted grains were bleached in a SOL2 solar simulator for 24 h.

An automated Risø TL/OSL reader (DA-20) equipped with a $^{90}\text{Sr}/^{90}\text{Y}$ beta source for irradiation, delivering a dose rate of ~ 0.08 Gy/s, was used for all luminescence measurements. A 150 mW 830 nm centred IR laser stimulated the grains, and the blue emission (~ 410 nm) was detected through a combination of two 2 mm Schott BG-39 filters and a 3 mm Corning 7-59 glass filter. A dose-rate map (Lapp et al., 2012), created by using radiosensitive film (GAF), showed a dose uniformity across the sample area of ~ 4.5 %. It is thus not expected to significantly contribute to the received doses of each grain. A dose recovery test (DRT, given dose = 150 Gy) was carried out employing a pIRIR protocol (Thomsen et al., 2008) with a preheat of 200 °C for 60 s and a pIRIR stimulation temperature of 175 °C (Madsen et al., 2011; Reimann et al., 2011). The IR₅₀ and pIRIR₁₇₅ measurement times were 2 s and 3 s, respectively. For further details on the single-aliquot regenerative-dose (SAR) DRT protocol used see Table 2 (Reimann et al., 2017). All measurements were performed as dose recovery test using a given dose of 150 Gy. This allowed for direct comparison between the luminescence response of the samples. Furthermore, given the curvature of the dose response curve of the different samples, a dose of 150 Gy allowed for investigating the performance of the SGC in the non-linear, but non-saturation, part of the DRC.

For signal integration the first 0.2 s minus a background of the last 0.4 s of stimulation was used. Five discs à 100 grains were measured per sample. All D_e estimates and SGCs were derived using the numOSL R package (Peng et al., 2018) and the least-squares (LS)-normalisation approach following Li et al. (2016). A measurement error for the regenerative dose signal (L_x) and the corresponding test dose signal (T_x) of 2 % was used for calculations. Parameters used for growth curve fitting were: “exponential model”, “not forced through origin” and “using a weighted procedure”. Rejection criteria for the SAR and SGC approaches were as follows: test dose signal following natural dose measurement (T_n) > 3 sigma above background, relative standard error (RSE) of T_n ≤ 25 %, recycling ratio = unity ± 10 % for all available recycling points, recuperation ≤ 10 % of the natural signal, recuperation ≤ 10 % of the maximum regenerative-dose signal, figure-of-merits (FOM) ≤ 10 % (Peng and Li, 2017), reduced chi square ≤ 10 %. The numOSL R package uses the recycling ratio ± two times the standard error to check if the recycling ratio is within unity ± 10 %. The FOM, a measure of goodness-of-fit, is

calculated as follows: $\text{FOM} = \frac{\sum |y_i^o - y_i^f|}{\sum y_i^f} * 100$ (Balian and Eddy, 1977). D_e with a RSE above 50 % were rejected after their calculation. A dose value of 150 Gy was used for SAR dataset re-normalisation in the pickSARdata() function.

2.3. Geochemistry (SEM-EDX)

Following the luminescence measurements double-sided sticky tape, on one side attached to a glass microscope slide, was placed on the top side of the SG discs. The undersides of the SG discs were lightly tapped with a piezoelectric ultrasonic cleaner (vibration frequency 30 ± 3 kHz) to transfer the grains onto the tape. About 80 % of the grains were extracted on average. Prior to disc removal from the tape the location of the disc position holes was marked on the tape. Subsequently the grains were embedded in colourless two-component epoxy resin (Huntsman Araldite 2020), with position hole placement marked on the epoxy discs. The surfaces of the epoxy discs were sanded with a 1200 SiO₂ sandpaper and polished to ensure that no epoxy covers the grains. The major element chemistry of individual grains was determined on a Zeiss Sigma 300-VP scanning electron microscope (SEM) with an energy dispersive spectroscopy (EDX) attachment. The working distance was set to 8.5 mm. The aperture diameter of 60 μm and an accelerating voltage of 20 kV resulted in an output count rate of $\sim 45,000$ cps. The chemical composition of individual feldspar grains was calculated based on the nine elements O, Na, Mg, Al, Si, K, Ca, Ti and Fe through stoichiometry. Three out of five discs per sample were measured for their geochemical composition. For the samples ISM-7, LAGU-1-1 and MBT-I-2430 two discs were analysed.

2.4. Statistic

For data comparison Spearman rank correlations were used (Spearman, 1904), since they are nonparametric correlations and therefore less susceptible to outliers (Kendall et al., 1939; Zar, 2005). The results of a Spearman rank correlation, the Spearman's rank correlation coefficient (r_s), can range between -1 and 1, with -1 being a perfect negative correlation and 1 a perfect positive correlation. The closer the r_s value is to zero, the weaker the correlation. As there is no universally valid definition, we here define correlations with r_s values between 0 and ±0.2 as very weak, between ±0.2 and ±0.4 weak, between ±0.4 and ±0.6 moderate, between ±0.6 and ±0.8 moderate to strong and between ±0.8 and ±1 strong. The significance of a correlation was tested using the cor.mtest() function of the corrplot() package (Wei and Simko, 2023). This test results in p-values for each correlation pair. If the p-value is >0.05, the correlation is not significant. Spearman rank correlations have the disadvantage that they do not take uncertainties of individual values into account. Nevertheless, we think that this does not affect our conclusions. All errors given here for D_e values correspond to one standard deviation. Presented arithmetic means are always given with the corresponding standard error.

3. Standardised growth curve (SGC) application and modification

3.1. SAR and SGC

3.1.1. Procedure

To test the applicability of the SGC approach, first the dose response properties using the standard SAR approach were assessed. For further analysis the dataset was divided into two subsets, Atacama Desert (A) and external (X) samples (cf. Table 1). For each subset A and X one SGC was calculated using the numOSL R package and the rejection criteria mentioned in section 2.2. Since the Atacama Desert samples are of main interest for this research, the SGC for subset A is hereafter called SGC. The SGC for subset X is referred to as xSGC and only used for direct comparison between SAR and SGC D_e values of dataset X to check its validity. The

Table 2

Single-grain dose recovery test SAR measurement protocol. Heating rate for steps 2-4 and 6-8 2 °C/s.

Step	Treatment ^a	Observation
1	Given dose D _i	
2	Preheat, 60s at 200 °C	
3	IRSL, 2s at 50 °C	
4	IRSL, 3s at 175 °C	L _x
5	Given test dose D _t	
6	Preheat, 60s at 200 °C	
7	IRSL, 2s at 50 °C	
8	IRSL, 3s at 175 °C	T _x
9	Return to step 1	

^a given dose D_i [Gy]: 150, 0, 50, 150, 300, 500, 800, 0, 50, 150; test dose D_t [Gy]: 50.

xSGC will be used in following sections for D_e calculation of grains from dataset A (see Fig. 1). Following Li et al. (2015a) two SAR cycles are needed for the D_e calculation using an existing SGC. Besides the “natural” cycle (L_n/T_n), an additional regenerative cycle with a regenerative dose D_{r1} is required for the projection onto the existing SGC. According to Li et al. (2015a) the size of D_{r1} should be close to the expected size of the D_e . Our expected dose is 150 Gy, which equals the regenerative dose of regenerative cycles R3 or R9. Unfortunately, the L_x/T_x values of regenerative cycles R3 and R9 of accepted grains often showed large deviations from the fitted growth curves of up to 44 % (see Fig. 2). Consequently, we decided to use regenerative cycle R8 (50 Gy) as D_{r1} .

3.1.2. Results & discussion

When using the standard SAR approach 657 grains out of 5000 analysed grains (13.1 %) passed the rejection criteria and resulted in a D_e . Most of the grains (56.7 %) were rejected due to T_n signals below 3 σ above background. Another 15.6 % were rejected based on poorly-fitted growth curves and 11.6 % were rejected for a T_n with a RSE > 25 %. Three additional grains were rejected due to their D_e value having a RSE > 50 %. For details on rejected grains see Supplement Table S1. The mean of the remaining 643 D_e values was 128 ± 1.42 Gy, which corresponds to a dose recovery ratio (DRR) of 0.85 ± 0.01 . MBT-I-2430 was the sample giving the most D_e values (309 grains \approx 47.2 %) and PAG-6-4b the one with the least (1 grain = 0.15 %). From the Atacama Desert samples (subset A) merely 88 out of 2500 grains were accepted resulting in 87 D_e . Whereas from the external samples (subset X) 558 out of 2500 grains were accepted resulting in 556 D_e values. In each subset one sample was dominating the following results. In subset A grains from sample LAGU-1-1 make up 71.3 % of the total number of accepted grains. While in subset X 54.7 % of the accepted grains were from sample MBT-I-2430. The DRR of 0.89 ± 0.02 for subset A was slightly better than for subset X with a DRR of 0.85 ± 0.01 . The generally observed underestimation of the given dose could be due to the protocol not being suitable for all samples. We also considered changes in sensitivity during the first measurement cycle (see Kars et al., 2014), but we could not find any indication for this (data not shown). Further investigations of the underestimation were not within the scope of this study.

The Atacama Desert samples are of main interest for this research, thus only D_e calculations for subset A are discussed in the following sections. Since the rejection criteria for the SAR and SGC methods were the same, 88 grains from subset A were used for the SGC construction and subsequent D_e calculation using the constructed SGCs. The LS-normalisation reduced the scatter between the grains in dataset A (see Supplement Fig. S1). The D_e calculation with the SGC was possible for 87 out of 88 grains. The DRR of the remaining SGC-acquired D_e values was 0.84 ± 0.03 . For further details on D_e distributions Abanico plots are provided in Supplement Fig. S2. The overdispersion within the dose recovery D_e distribution calculated with the SAR approach and the SGC method was 19.4 ± 2.4 % and 19.6 ± 2.4 % respectively, which is in a typical range for single-grain pIRIR measurements (Brill et al., 2018; Reimann et al., 2012).

It has been shown that the validity of the SGC can be tested by comparing the SAR and SGC D_e values \pm their 2 σ standard error, which should be in unity (e.g., Li et al., 2015a,b; Sontag-González et al., 2021). For 86 grains D_e values were calculated with both methods and were used for the comparison. All 86 grains were in unity at 2 σ , therefore the SGC can be regarded as reliable.

When reporting luminescence ages the 1 σ standard error is commonly used (Mahan et al., 2022). The D_e values showed average RSEs of \sim 16 %, therefore the agreement within 1 σ seems inappropriate to evaluate the precision between the SAR procedure and the SGC method. Therefore, we focus on the number of grains differing less than \pm 10 % in their calculated D_e values (Fig. 1A) and on Spearman rank correlations. Of the 86 comparable grains, 41 D_e values did not differ more than \pm 10 %, 37 additional grains had indistinguishable D_e values at 1 σ and 8 additional grains exhibited D_e values within 2 σ . SAR and

SGC results correlate with a r_s of 0.81, which can be regarded as the lower limit of a strong correlation.

Comparing the SGC and SAR D_e values, all 86 grains yielding a D_e value with the standard SAR procedure and the SGC approach are in unity within 2 σ . However, only a low number of these grains yield D_e values with a good precision. There are several reasons why the SGC approach estimates D_e values which do not agree within \pm 10 % with the SAR method. Firstly, the dataset for constructing the SGC is very small ($n = 88$). Secondly, even though D_{r1} was chosen to reduce the influence of odd L_x/T_x values, some L_{r1}/T_{r1} still showed deviation from the growth curve of up to 35 %. Thirdly, the overall large RSE of the dataset indicates poor luminescence properties.

3.2. External SGC (xSGC)

3.2.1. Procedure

In future studies it seems more likely to use an already established SGC rather than constructing a SGC for every new sampling site. Therefore, the established SGC might be constructed from samples with different geographical and geological origin than the samples it is used for. To mimic this scenario, we test the performance of the xSGC, constructed with subset X, to analyse subset A. The xSGC was constructed in the same manner as the SGC (see section 3.1.1). For shape of the xSGC see Fig. S1. To test the validity of the xSGC the D_e values for dataset X acquired with the SAR method and the xSGC where compared. Out of 555 comparable grains 554 were in unity at 2 σ , therefore the xSGC can be regarded as reliable (e.g., Li et al., 2015a,b). For the subsequent D_e calculation of dataset A the parameters of the xSGC were used in the calSGCED() function.

3.2.2. Results & discussion

Next the D_e results using the SGC and xSGC are compared in the same manner as SAR and SGC above (Fig. 1B). Using the xSGC, D_e values for all 88 grains could be calculated. A total of 87 mutual grains were used for the comparison between SGC and xSGC. All but one of them agreed within less than \pm 10 %. If the SGC D_e is considered to be the true D_e , xSGC D_e s all slightly underestimated with an average of 4.14 ± 0.56 Gy. The large uncertainty is caused by one grain not being within \pm 10 % in unity. The correlation between both D_e results is perfect with a r_s of 1. The one grain, which differed slightly more than 10 %, is still in agreement if the 1 σ errors of the two D_e values are considered (cf. Fig. 1B). This particular grain had an L_x decay curve in the eighth regenerative cycle (R8) with an unusual low net signal and a relatively high background. SGC and xSGC calculated unusually high D_e values based on this one L_x/T_x . With D_e values of 345 ± 151 Gy for the SGC and 298 ± 93 Gy for the xSGC, they were around twice as high as the given dose of 150 Gy. For comparison the SAR D_e for this particular grain was 198 ± 40 Gy, which demonstrates that outliers in individual measurement cycles can have a considerable effect on the SGC results if the outliers occur in the D_{r1} cycle.

In general, the deviation between D_e derived with the different SGCs increases with increasing L_n/T_n . As with the D_e calculation using a SAR growth curve, small changes in L_n/T_n result in larger changes in the D_e the closer to saturation they intersect the growth curve. L_n/T_n above $2D_0$ are therefore usually not considered (Murray et al., 2002).

The agreement between SGC and xSGC results confirms Li et al. (2015b) findings, that a ‘global SGC’ is suitable for feldspar samples and Mueller and Preusser (2022) observations that SGC results are not biased if the same input grains are used for SGC construction and application. In our future studies in the Atacama and elsewhere, the case of using a xSGC seems more likely because it is created with a larger dataset and might thus be more robust. Since the correlation between SGC and xSGC D_e values is perfect, all further data is generated with the xSGC.

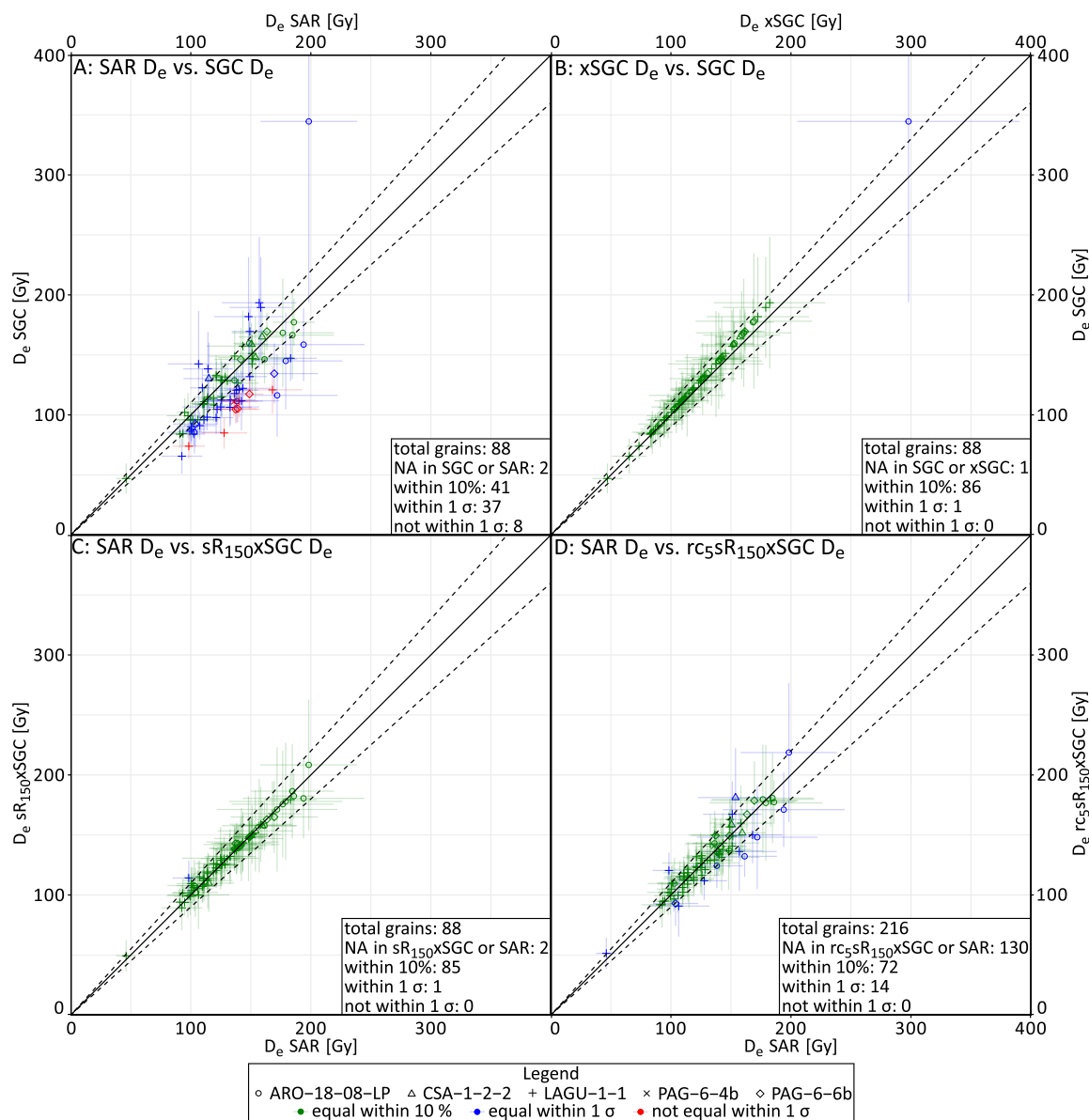


Fig. 1. Evaluation of SGC performance. **A)** comparison of D_e from samples of subset A (Table 1) obtained by the standard SAR procedure with D_e obtained using a SGC established with the same measurements, fitted with their L_{r1}/T_{r1} from the eighth regenerative SAR cycle with a D_{r1} of 50 Gy (Table 2); **B)** comparison of D_e from samples of subset A obtained by a SGC, established using the same samples, and obtained by a xSGC, constructed with data from subset X (Table 1); **C)** comparison of D_e from samples of subset A obtained by the standard SAR procedure with D_e obtained using the xSGC from B) and fitting the individual grains with L_{sR}/T_{sR} from an synthetic cycle with a D_{r1} of 150 Gy (sR₁₅₀xSGC); **D)** comparison of D_e from samples of subset A obtained by the standard SAR procedure with D_e obtained using the sR₁₅₀xSGC from C) and reducing the SAR-cycles for individual growth curve fitting to the “natural” 150, 0, 50, 500, 50 Gy cycles (rc₅sR₁₅₀xSGC).

3.3. Synthetic R (sR)

3.3.1. Procedure

When fitting a SAR growth curve using any function, in our case a single saturating exponential, all L_x/T_x points measured are considered by the fit. However, when interpolating data onto a constructed SGC only the natural signal and one regenerative dose point are used (Li et al., 2015a). Thus, in their original approach only those two cycles were measured for D_e estimation. We tested this approach and removed all measurement cycles from our dataset except for the “natural” signal and regenerative cycle eighth (R8 = 50 Gy). Therefore, only the rejection criteria $T_n > 3$ sigma above background, relative standard error (RSE) of $T_n \leq 25\%$ and RSE of the D_e above 50% could be applied. From the analysed 2500 grains from dataset A, 243 passed these rejection criteria

(see Supplement Table S2). Out of those 243 grains three grains were classified as saturated by the calSGC() function. The remaining 240 grains resulted in a finite D_e value, from which 86 D_e values could be compared to the D_e values achieved with the standard SAR approach. Although all 86 comparable grains were in unity within 2 σ , we were not satisfied with the performance. As Fig. S3 shows, the precision of the comparable D_e values was about the same as in chapter 3.1 and the scatter in the not comparable grains was large. However, the mean D_e value of the not comparable grains is in unity within 1 σ with the mean D_e value of the SAR approach.

If we would not have measured the full SAR cycle, we would not have known, that R8 has fewer odd L_x/T_x values than R2 and R3. As mentioned in section 3.2.2 odd individual L_x/T_x values used as L_{r1}/T_{r1} can lead to pronounced over- or underestimation of the D_e values, when

these values deviate significantly from the fitted growth curve (cf. Fig. 2A). The grain depicted in Fig. 2A for example passed all rejection criteria and had a D_e value of 154 ± 31 Gy calculated with the standard SAR approach. Using R8 as L_{r1}/T_{r1} it had a D_e of 142 ± 31 Gy. Using either R2 or R3 as L_{r1}/T_{r1} the D_e values were estimated at 308 ± 89 Gy and 92.7 ± 19.9 Gy (cf. Fig. 2B). Due to the large errors they still agree with the SAR D_e with unity at 2σ .

We therefore introduce a new parameter and procedure for the projection of multiple L_x/T_x onto the constructed SGC. This parameter should ideally overcome the problem of including grains with unsuitable luminescence characteristics (e.g. too large recycling ratios or FOM >10%) and furthermore reduce the effect of odd individual L_x/T_x values. Instead of using a single L_x/T_x point as L_{r1}/T_{r1} we chose a L_x/T_x point, which we extracted from the fitted growth curve. We term this point synthetic regenerative dose (sR). For this we used the growth curves of each grain and reversed the process of D_e estimation from a growth curve. We chose an sR, for example 200 Gy (cf. Fig. 2A), and inserted it into our exponential function (eq. 1). Thereby we projected the sR onto the growth curve whereby we calculated the point of interception with the growth curve to get the value on the y-axis of our synthetic L_{sR}/T_{sR} (Fig. 2).

$$\text{(eq. 1)} \quad \frac{L_{sR}}{T_{sR}} = a^* (1 - \exp(-sR^b)) + c$$

With a, b and c being the parameters a, b and c from the grain-wise exponential growth curve, calculated during the normal SAR procedure and sR a value in Gy. L_n/T_n and L_{sR}/T_{sR} were then used as input parameters for the function calSGCED() to calculate the D_e values.

To evaluate if there is an influence of the size of sR on the resulting D_e and DRR we tested eight different sR values: sR₅₀, sR₁₀₀, sR₁₂₅, sR₁₅₀, sR₁₇₅, sR₂₀₀, sR₃₀₀ and sR₈₀₀, with the subscript being the size in Gy.

3.3.2. Results & discussion

The results were evaluated in the same manner as SAR and SGC in section 3.1.1 based on a comparison of D_e and DRR results of the SAR procedure and the sR₅₀₋₈₀₀xSGC procedures. For detailed results of all sR tested see Supplement Table S3). For all sR sizes, except for 800 Gy, 86 D_e values for the 88 not rejected grains were calculated. With sR₈₀₀ 87 D_e values were calculated. Since sR₁₀₀, sR₁₂₅ and sR₁₅₀ had the most grains within 10 % in unity with the SAR results, the other five sR values will not be discussed further. With sR₁₂₅ all grains had D_e values within 10 % in unity with the SAR D_e values, whereas sR₁₅₀ had one and sR₁₀₀ three grains not within 10 %. With DRRs of 0.86 ± 0.02 , 0.87 ± 0.02 and 0.89 ± 0.02 for sR₁₀₀, sR₁₂₅ and sR₁₅₀ respectively all three sR procedures showed an improved DRR compared to the above presented conventional SGC approach (0.84 ± 0.03). The correlation between the SAR D_e values and those achieved with sR₁₀₀, sR₁₂₅ and sR₁₅₀ was strong positive with Spearman's rank correlation coefficient (r_s) of 0.99 for all three sR values tested. The differences between sR₁₀₀, sR₁₂₅ and sR₁₅₀ were small, with sR₁₂₅ having the most D_e results equal within 10 % with the SAR procedure but sR₁₅₀ yielding the better DRRs.

Deviations of sR from the expected D_e (here 150 Gy) of ~30 % (± 50 Gy), do not cause major alterations in the D_e results in this data set. All sR ranging from 100 to 200 Gy have a strong positive correlation with the SAR procedure, with a minimum r_s of 0.94. In comparison with the SAR data, if the sR was slightly smaller than the expected D_e (sR_{100,125}), the method yielded better results than if the sR was slightly larger (sR_{175,200}). A cause for the better agreement with the SAR results might be the overall underestimation of the D_e with the SAR procedure. Since the differences between the best performing sR were very small and the sR₁₅₀ had the same DRR as the SAR procedure, we chose an sR of 150 Gy for our further analysis (see Fig. 1C). Furthermore, the sR₁₅₀ equals the recommended size for a D_{r1} (Li et al., 2015a). We therefore conclude that sR should be chosen to be the same size as the expected D_e . Nevertheless, considering that the D_e is normally unknown before measurement, it is reassuring that choosing an

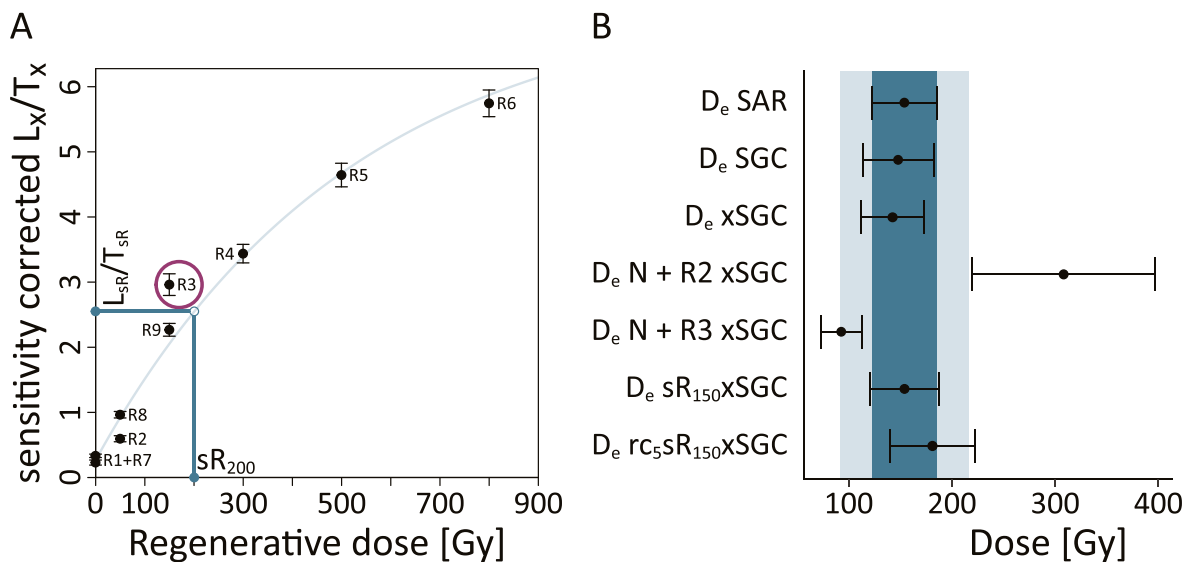


Fig. 2. Influence of odd L_x/T_x values and the mitigation strategy of implementing (sR) A) Process of L_{sR}/T_{sR} determination with an sR of 200 Gy on an example exponential SG growth curve of the sample CSA-1-2-2 with an odd L_x/T_x value in the third regenerative SAR cycle ($D_i = 150$ Gy). The vertical line from the X-axis towards the growth curve illustrate the process of calculating the interception. The horizontal line from the growth curve towards the Y-axis illustrate the subsequent determination of L_{sR}/T_{sR} . B) Comparison of D_e values of the same grain estimated using different techniques with: SAR using the standard SAR approach, SGC using the SGC constructed with data from subset A and regenerative cycle R8 (50 Gy) used for projection onto the SGC, xSGC using the xSGC constructed with data from subset X and regenerative cycle R8 used for projection onto the xSGC, N + R2 xSGC using only the natural and regenerative cycle R2 (50 Gy) for the rejection process and using the xSGC constructed with data from subset X and regenerative cycle R2 used for projection onto the xSGC, N + R3 using the same procedure as N + R2 but using R3 (150 Gy) instead of R2, sR₁₅₀xSGC using the same procedure as xSGC but instead of using R8 for projection onto the SGC the sR method with a sR of 150 Gy was used, rc₅sR₁₅₀xSGC (introduced in chapter 3.4) is using only regenerative cycles N, R1, R2, R4 and R8 (cf. Table 3) for the rejection process and the sR method with a sR of 150 Gy for projection onto the xSGC.

sR value within 30 % of the natural dose does not seem to have too great of an effect on final D_e calculations.

3.4. Reduction of SAR cycles (rc)

3.4.1. Procedure

Whilst the sR approach helps in making the interpolation onto the SGC more robust, it still requires the construction of a full growth curve for every grain and thus not saving any measurement time. Here we test which cycles can be removed to save time while still yielding robust D_e values with the sR₁₅₀xSGC method. We carried out ten different reduced cycle (rc) scenarios, all containing the “natural” cycle and a zero-dose cycle (recuperation). Besides these two cycles, we tested if two additional cycles are enough to incorporate the sR method or if a third cycle, a recycling point, is needed as well. We also investigated which dose size yielded the best results. For the recycling point we could only test 50 Gy and 150 Gy since those were the only recycling doses in our SAR protocol. The ten tested rc scenarios are listed in Table 3 and afterwards abbreviated with their test number according to Table 3 as a subscript. The dataset used for xSGC establishment was not reduced.

3.4.2. Results & discussion

Reducing the number of SAR cycles used led to an increase of accepted grains, with fewer grains being rejected due to their poor growth curve fitting compared to when using full SAR cycles. For detailed rejection criteria and results of all tested rc see Supplement Tables S4 and S5.

The growth curves produced in rc_4 used for the sR method are not reliable since the highest given dose used for their calculation is still in the linear part of the growth curves constructed with the full set of SAR cycles. Many grains were falsely excluded as they appeared to be saturated. Furthermore, the results did not agree with the SAR procedure (see Table S4), thus rc_4 is not discussed further. All other tested rc were able to calculate ~200 D_e values out of the 2500 measured grains. In a direct comparison to the SAR D_e values, all nine remaining tested rc had at least 85 common grains with the SAR results. All showed similar results (see Table S5) with rc_5 and rc_6 showing the best performance. The other seven rc approaches are therefore not discussed further.

rc_5 and rc_6 had the same setup for the cycle reduction, with remaining cycles being the “natural” cycle, a zero-dose cycle, a recovery dose of 50 Gy plus one additional dose. The additional doses of 300 Gy and 500 Gy, respectively, are between D_0 (284 Gy) and $2D_0$ (568 Gy) of the xSGC. rc_6 was able to calculate eight D_e more than rc_5 but rc_5 had the best overall results. With rc_5 197 D_e values were calculated, of which 72 were equal with the SAR results within $\pm 10\%$ and the remaining 14 D_e were identical within the 1σ error (cf. Fig. 1D). The mean difference between the D_e values was 7.40 ± 0.70 Gy and the DRR of rc_5 was 0.9 ± 0.02 , which is in unity within 1σ with the SAR-achieved DRR of 0.89 ± 0.02 .

Compared to the approaches described in section 3.1 and 3.2 (e.g. using the full SAR measurement for the rejection process and R8 for the projection onto the SGC or xSGC), the accuracy and the precision of

Table 3

Reduced cycle scenarios tested for subset A. The full SAR protocol used is given in Table 2.

Abbreviation	Used cycles	D_i of used cycles [Gy]
rc_1	N + R1 + R2 + R4	150 + 0 + 50 + 300
rc_2	N + R1 + R2 + R5	150 + 0 + 50 + 500
rc_3	N + R1 + R2 + R6	150 + 0 + 50 + 800
rc_4	N + R1 + R2 + R3 + R8	150 + 0 + 50 + 150 + 50
rc_5	N + R1 + R2 + R4 + R8	150 + 0 + 50 + 300 + 50
rc_6	N + R1 + R2 + R5 + R8	150 + 0 + 50 + 500 + 50
rc_7	N + R1 + R2 + R6 + R8	150 + 0 + 50 + 800 + 50
rc_8	N + R1 + R3 + R4 + R9	150 + 0 + 150 + 300 + 150
rc_9	N + R1 + R3 + R5 + R9	150 + 0 + 150 + 500 + 150
rc_{10}	N + R1 + R3 + R6 + R9	150 + 0 + 150 + 800 + 150

the D_e values achieved with the rc_5 sR₁₅₀xSGC compared to the D_e values estimated using the SAR procedure improved (cf. Fig. 1 and Supplement Fig. S2). The scatter in the D_e values not comparable with SAR results was smaller using rc_5 sR₁₅₀xSGC than using the natural and one additional L_X/T_X value for the rejection process and the projection onto the xSGC (cf. Supplement Fig. S3). The mean D_e value of the not comparable grains was in unity within 1σ with the mean D_e value of the SAR approach. All the grains yielding those extra D_e values, were rejected due to a FOM >10 % when using the full SAR procedure during the rejection process. Since the extra rc_5 sR₁₅₀xSGC D_e values are in the same range and showing similar scatter as the rest of the rc_5 sR₁₅₀xSGC D_e values which are comparable to the SAR results, we assume that those additional D_e values can be regarded as reliable.

Compared to the correlation of the sR₁₅₀xSGC results, with a r_s of 0.99, the correlation of the rc_5 sR₁₅₀xSGC and the SAR approach is worse with a r_s of 0.94. Nevertheless, the rc_5 sR₁₅₀xSGC is still an improvement compared to the conventional SGC approach ($r_s = 0.81$, DRR = 0.84 ± 0.03). Furthermore, it is possible to estimate more than twice as many D_e , resulting in fewer discs to be measured. The reduction of measurement cycles saves approximately 60 % of measurement time per disc.

We therefore recommend applying the $rcsRxSGC$ approach when dealing with problematic single grain feldspars, with an sR in the size of the expected D_e and a rc scenario with a recuperation point, a recycling point - smaller than the expected D_e , and an additional dose point with a size of D_0 to $2D_0$ of the SGC used. If this approach is also applicable for expected D_e values with sizes greater than $2D_0$ needs to be evaluated.

3.5. Dose recovery ratio (DRR)

Since our dataset is based on a dose recovery test, another measure to test the performance of our approach is the dose recovery ratio. Overall, the given dose of 150 Gy is underestimated by all applied methods, including the standard SAR procedure. Fig. 3 shows a comparison of the D_e results achieved with the SAR procedure and the rc_5 sR₁₅₀xSGC method. With the SAR procedure, 52 out of 87 grains yield a DRR within 1 ± 0.1 if their 1σ errors were considered and 35 grains differed more than ± 0.1 from a DRR of 1 even when their 1σ errors were considered. Out of the 197 D_e values calculated using the rc_5 sR₁₅₀xSGC method, 134 grains had a DRR of 1 ± 0.1 if their 1σ errors were considered and 63 D_e values differed more than ± 0.1 from a DRR of 1 even when their 1σ errors were considered. Thus, using the rc_5 sR₁₅₀xSGC method we observed a higher percentage of grains yielding a DRR within the desired 1 ± 0.1 , contributing to an overall improved DRR.

4. Single grain geochemistry (SEM-EDX)

4.1. Procedure

The SEM-EDX measurements were carried out at the Institute of Geology and Mineralogy of the University of Cologne, by defining regions of interests on the polished grain surfaces. These regions of interest were than mapped with a pixel size of 2 μm , resulting in average values for each region of interest. The elemental analysis results of each measured region were assigned to the individual grains on the basis of the maps of the measurements. Unfortunately, SEM-EDX data could not be obtained for every grain. Some grains got lost during the transfer process from the discs to the tape, the position of others was slightly altered during embedding them in epoxy. If a grain was subsequently not clearly identifiable, its SEM-EDX results were not considered. For some grain positions (i.e., holes in the discs) more than one SEM-EDX result was obtained. This was either due to multiple grains being located in one hole or due to breaking of the grains during the transfer process. For grains and holes with more than one SEM-EDX measurement result, the average was calculated.

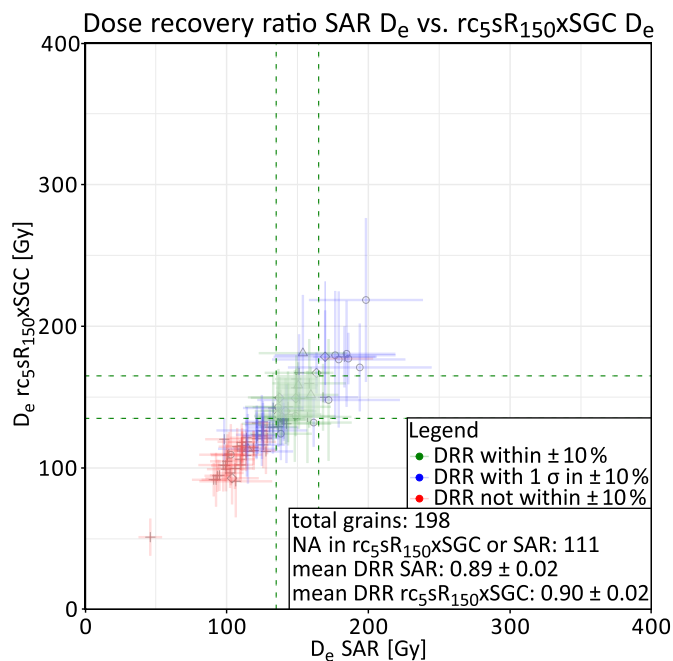


Fig. 3. D_e values from grains of subset A, calculated with the standard SAR procedure (x-axes) and the $rc_5sR_{150} \times SGC$ method (y-axes). Colours of the horizontal and vertical 1σ error bars represent if the DRR calculated with SAR or $rc_5sR_{150} \times SGC$ are within unity $\pm 10\%$ (green), within $1 \pm 10\%$ if the 1σ error is considered (blue) or if they are not within $1 \pm 10\%$. Shape of the datapoints indicates the sample allocation (cf. legend Fig. 1).

4.2. Results

The results for the nine analysed elements are summarised in Fig. 4, for detailed measurement results see Supplement Table S6. 2328 grains, out of the 5000 grains analysed for their luminescence characteristics, could be clearly identified on the SEM-EDX maps. From those 2328 grains, 250 gave suitable luminescence signals for D_e calculation with the SAR procedure and 492 with the $rc_5sR_{150} \times SGC$ method. Those grains are hereafter called luminescent grains. All luminescent grains from subset A ($n = 65$) contained O, Na, Al, Si and K, implying that no luminescent grain from the Atacama Desert was pure orthoclase. About half of them also contained Ca and Fe. From subset X ($n = 434$) most of the grains (>400) were also composed of O, Na, Al, Si and K, with 200 of them also having Ca and 15 of them being pure orthoclase, based on their geochemical composition.

The K-content of all luminescent grains varied between 0.06 wt% and 14.6 wt%, with a mean value of 7.04 ± 0.26 wt%. The coefficient of variation of all luminescent grains of 80 % indicates that luminescent grains can have a wide range of K-contents, supporting the findings from O’Gorman et al. (2021) and Zinelabedin et al. (2022). The SEM-EDX results presented in Fig. 4 suggest that there is no clear difference between the geochemical composition of luminescent and non-luminescent grains, neither for subset A nor subset X. Although, for example the median K-content of luminescent grains is higher than the median K-content of non-luminescent grains, this does not imply that all grains with low K-contents do not emit suitable luminescent signals nor that all grains with high K-content emit suitable luminescent signals.

5. Correlation of luminescence characteristics and geochemistry

To evaluate whether signal intensity and K-content are linked and if there are further relationships within and between geochemistry and luminescence properties, we created nine correlation matrices. We performed Spearman rank correlations for the entire dataset and the two subsets. We then calculated six correlation matrices for these three

categories by dividing them in luminescent and non-luminescent subgroups. In addition to the nine elements from the SEM-EDX analysis, the following luminescence properties were used as input variables: D_e and DRR determined with SAR, D_e and DRR determined by $rc_5sR_{150} \times SGC$, to check whether high or low D_e or DRR are linked to geochemistry or signal intensity, L_n and T_n , to check whether there is a correlation between brightness of the grain and geochemistry. For better readability, only the correlation matrix of the entire data set is shown in Fig. 5. The eight remaining correlation matrices can be found in Supplement Fig. S4.

No strong or moderate to strong correlation could be observed between any element and luminescence characteristics if the entire dataset is considered, as can be seen inside the blue square in Fig. 5. This also holds true regardless of whether the subset data or subgroups of the entire or subset data are considered. Furthermore, $\sim 47\%$ of those correlations have a p-value >0.05 and are therefore not considered significant. The most significant correlation between SEM-EDX results and luminescence is the negative correlation observed between the Fe-content and the signal intensity (L_n and T_n) in the correlation matrix of all grains from subset X with a r_s of -0.57 and -0.56 for L_n and T_n respectively. The correlation between Fe-content and signal intensities in subset A is also negative but only very weak or weak, if significant at all. There is no significant correlation between K-content and the signal intensity (L_n and T_n) in subset A when only the luminescent grains are considered, but a weak negative correlation can be found in subset X. In contrast, the same correlation for the non-luminescent grains is very weak to weak positive in both datasets. In Fig. 5 these correlations between K-content and L_n respectively T_n are weak and very weak positive, since a greater number of non-luminescent grains contribute to the overall correlation in Fig. 5 (cf. Table S6). Conversely, Na and Ca contents show a positive correlation with the signal intensity in the luminescent grains and a negative correlation in the non-luminescent ones (Figs. S4B and C).

Within the luminescence characteristics there is no strong significant correlation between the signal intensity and the D_e or the DRR. Since the D_e values and DRRs determined with the same method have a perfect correlation, all correlations between D_e s and DRRs determined with different methods yield the same r_s values within each correlation matrix. For subset A the r_s of these correlations is 0.94, for subset X and for both subsets combined it is 0.93. The correlation between L_n and T_n is almost perfectly positive if only the luminescent grains are considered, but substantially weaker if all or just non-luminescent grains are correlated. Within the geochemical data the correlation values between the nine correlation matrices vary to a greater extent than within the luminescence characteristics. Correlations found between different elements reflect the general chemical characteristics of the feldspar mineral group, with Si:Al ratios differing between alkali feldspars and plagioclase and with a known miscibility gap between K- and Ca-feldspars. The strong negative correlation between Si and Al contents is particularly pronounced when only the non-luminescent grains are considered, but visible in all nine matrices. When only the luminescent grains are considered the correlations between K and Na as well as K and Ca contents are moderate to strong negative, while the correlations between Na and Ca contents are moderate or very strong positive. None of the K-, Na- and Ca-content correlations is more than moderate in the non-luminescent correlation matrices but all are in the same directions as in the luminescent grains.

The luminescent grains from sample ARO-18-08-LP have a very strong negative correlation of -0.83 and -0.86 between their Fe-contents and the signal intensities L_n and T_n . Zinelabedin et al. (2022), investigating the same samples, suspected that the high Fe-contents might be caused by Fe-rich coatings of the feldspar grains. These iron layers around the sediment grains could on the one hand explain the high Fe-content of up to 8.8 % in luminescent grains and on the other hand the observed low luminescence intensities, since Fe coatings could cause absorption of the emitted luminescence (Kook et al., 2011). Geake

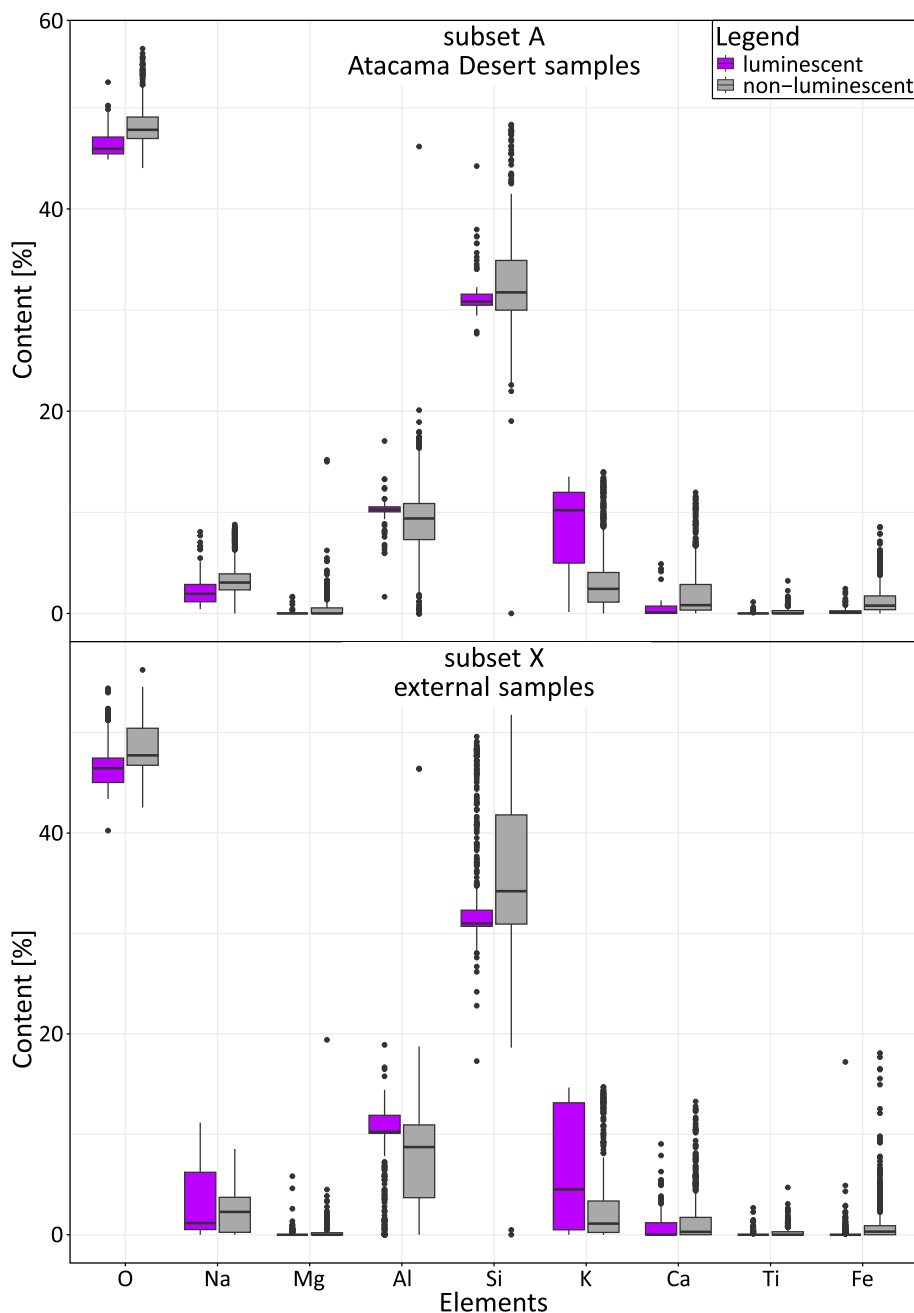


Fig. 4. Statistical distribution of all measured element concentrations for A) the grains from subset A and B) the grains from subset X grouped into luminescent (purple) and non-luminescent grains (gray). The lower and upper hinges correspond to the first and third quartiles (the 25th and 75th percentiles). The upper whisker extends from the hinge to the largest value no further than $1.5 \times$ IQR from the hinge (where IQR is the inter-quartile range, or distance between the first and third quartiles). The lower whisker extends from the hinge to the smallest value at most $1.5 \times$ IQR of the hinge. Data beyond the end of the whiskers are called "outlying" points and are plotted individually. The horizontal bar represents the median.

et al. (1972) and Finch and Klein (1999) present alternative explanations for the negative correlation between Fe-content and L_n and T_n intensities. Ultimately, we cannot give a satisfactory explanation of the observed negative correlation between Fe-content and luminescence intensity at this stage. The previously reported and generally accepted relationship of K-content and luminescence signal intensity is not supported by our data. The non-existing correlation between K-content and signal intensity in subset A confirms the findings of O'Gorman et al. (2021) and thereby falsifies the common hypothesis of a positive correlation (e.g., Huntley and Baril, 1997; Prescott and Fox, 1993; Spooner, 1992) at least for our set of samples. The weak negative correlation in subset X is further evidence that a higher K-content is not the main

determinant for a high signal intensity.

6. Conclusion

Atacama Deserts feldspars are challenging for single grain luminescence measurements for two reasons: firstly, only a small percentage of grains emits satisfactory luminescence signals (on average 3.52 %) and secondly their geochemical compositions are highly variable (on average 3.40 wt% K). To obtain a sufficient number of accepted grains for palaeodose calculation, numerous discs have to be measured, resulting in a long overall measurement time. We therefore tested the application of the standardised growth curve (SGC) method (Li et al.,

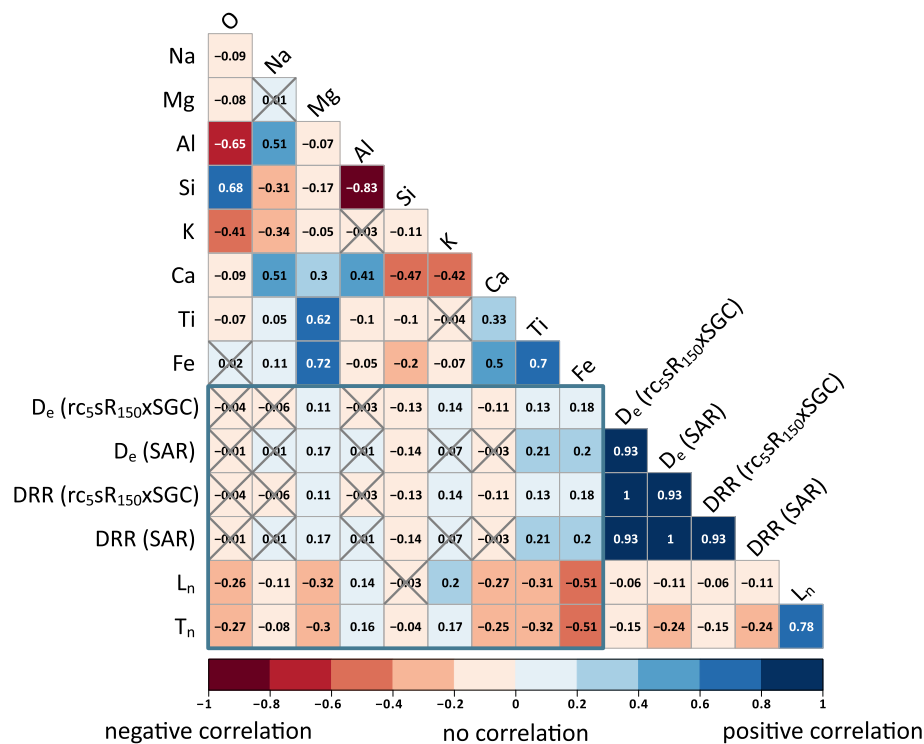


Fig. 5. Correlation matrix of the complete dataset (subset A + X). Numbers in the squares represent Spearman's rank correlation coefficient values and their colour the strength of the correlation. For not significant correlations with a p-value above 0.05 % the squares are crossed out. The turquoise square surrounds the correlation between the geochemical data and the luminescence characteristics.

2015b) with a dose recovery test using a pIRIR₁₇₅ protocol on ten chemically different feldspar sediment extracts. With a perfect correlation between SGC and xSGC results, we confirmed that the geographical and geological origin of the samples, for which the D_e is estimated, can differ significantly from the geographical and geological origin of the samples used for SGC construction and that the SGC is not biased if the same input grains are used for SGC construction and application.

We introduced a new and more robust method for interpolation of L_x/T_x values onto the SGC. The new sR (synthetic regenerative dose) method, reduces the influence of odd individual L_x/T_x values on the interpolation and D_e calculation. With the sR method a synthetic L_x/T_x , based on the growth curves of the individual grain, is used for D_e calculations with the SGC method. Since the sR method relies on the individual growth curves, no measurement time is saved. Therefore, we further tested how to reduce regenerative cycles to obtain a suitable growth curve for the sR method. With our new established rcsRxSGC method we were able to reduce our measurement time per disc by ~60 %. Furthermore, we were able to calculate around twice as many D_e per disc with the rcsRxSGC method than with the SAR procedure. Thus, potentially more measurement time can be saved, since fewer discs need to be measured to gain a sufficient amount of suitable grains.

We investigated the relationship of K-content and luminescence characteristics, as well as their implications for internal dose rate determination. Therefore, we measured the geochemical composition of the grains previously analysed for their luminescence properties using a costly and time-consuming scanning electron microscope (SEM) with energy-dispersive X-ray spectroscopy (EDX) attachment. Since no correlation between the K-contents and luminescence properties could be found, we conclude that for single grain measurements in feldspars with heterogeneous K-contents the internal dose rate estimation should not be based on an average literature-based value. Further, we cannot recommend using SEM-EDX measurements to overcome the problem, since they are costly and time consuming. Therefore, the internal dose rate determination for single grain luminescence measurements remains

a challenge.

When dealing with geochemically heterogeneous feldspars which give few suitable luminescence signals during single grain pIRIR measurements, we recommend using the rcsRxSGC method with an sR in the size of the expected D_e and rc consisting of a recuperation point, a recycling point with a size smaller than the expected D_e , and an additional dose point with a size of D_0 to $2D_0$ of the xSGC. Yet a feasible solution for single grain K-content measurements is still needed.

CRedit authorship contribution statement

Linda A.E. Mañon: Writing – review & editing, Writing – original draft, Visualization, Software, Methodology, Investigation, Formal analysis, Data curation. **Svenja Riedesel:** Writing – review & editing, Supervision, Methodology, Investigation, Conceptualization. **Anja Zander:** Writing – review & editing, Methodology, Investigation. **Mariana Sontag-González:** Writing – review & editing, Software, Methodology, Investigation, Conceptualization. **Tony Reimann:** Writing – review & editing, Supervision, Methodology, Investigation, Funding acquisition, Conceptualization.

Declaration of competing interest

The authors declare that they have no known competing financial interests or personal relationships that could have appeared to influence the work reported in this paper.

Data availability

Data will be made available on request.

Acknowledgements

This project is affiliated to the Collaborative Research Centre (CRC)

1211 “Earth – Evolution at the Dry Limit” (Grant-No.:268236062) funded by the German Research Foundation (Deutsche Forschungsgemeinschaft, DFG), Germany. We would like to thank our colleagues who kindly supplied us with sample material. We thank Georgina E. King (Université de Lausanne) for MBT-I-2430, Benny Guralnik (Technical University of Denmark) for KTB-383-C, Dominik Brill (University of Cologne) for PAG-6-4b, PAG-6-6b and ISM-7, Simon M. May (University of Cologne) for CSA-1-2-2 and LAGU-1-1 and Aline Zinelabedin (University of Cologne) for ARO-18-08 LP. SR would like to thank Ulrike Hardenbicker for guidance in the field during which sample ABLR-1 was taken, and for hosting her at the University of Regina,

Canada. We also thank Kathrin Jung (University of Cologne) for embedding our grains in resin and Hanna Cieszynski (University of Cologne) for the SEM-EDX measurements. SR acknowledges support by the European Union’s Horizon Europe research and innovation programme under the Marie Skłodowska-Curie grant agreement (RECREATE, grant no.101103587) during co-writing and editing the manuscript. The sampling campaign during which sample ABLR-1 was sampled was financially supported by a Female Research Grant from the Faculty of Mathematics and Natural Sciences, University of Cologne, awarded to SR.

Glossary

dataset A	dataset built with five samples from the Atacama Desert (cf. Table 1)
dataset X	dataset built with five samples from outside the Atacama Desert (cf. Table 1)
D_i	regenerative dose
D_{r1}	regenerative dose from which the L_x/T_x value is used for fitting onto the SGC
L_{sR} and T_{sR}	synthetic L_{r1}/T_{r1} signal used for fitting onto the SGC
L_{r1} and T_{r1}	signal and test dose signal used for fitting onto the SGC
rc	reduced measurement cycles
rcsRxSGC	SGC built with dataset X and data from A with reduced cycles and synthetic regenerative dose used for fitting
r_s	Spearman rank correlation coefficient
SGC	standardised growth curve
sR	synthetic regenerative dose
xSGC	SGC built with dataset X

Appendix A. Supplementary data

Supplementary data to this article can be found online at <https://doi.org/10.1016/j.quageo.2024.101585>.

References

- Amundson, R., Richter, D.D., Humphreys, G.S., Jobbágy, E.G., Gaillardet, J., 2007. Coupling between biota and Earth materials in the critical zone. *Elements* 3, 327–332. <https://doi.org/10.2113/gselements.3.5.327>.
- Balian, H.G., Eddy, N.W., 1977. Figure-of-merit (FOM), an improved criterion over the normalized chi-squared test for assessing goodness-of-fit of gamma-ray spectral peaks. *Nucl. Instrum. Methods* 145, 389–395. [https://doi.org/10.1016/0029-554X\(77\)90437-2](https://doi.org/10.1016/0029-554X(77)90437-2).
- Bartz, M., Duval, M., Brill, D., Zander, A., King, G.E., Rhein, A., Walk, J., Stauch, G., Lehmkühl, F., Brückner, H., 2020a. Testing the potential of K-feldspar pIR-IRSL and quartz ESR for dating coastal alluvial fan complexes in arid environments. *Quaternary International*, Electron spin resonance (ESR) dating in Quaternary studies: evolution, recent advances and applications 556, 124–143. <https://doi.org/10.1016/j.quaint.2020.03.037>.
- Bartz, M., Walk, J., Binnie, S.A., Brill, D., Stauch, G., Lehmkühl, F., Hoffmeister, D., Brückner, H., 2020b. Late Pleistocene alluvial fan evolution along the coastal Atacama Desert (N Chile). *Global Planet. Change* 190, 103091. <https://doi.org/10.1016/j.gloplacha.2019.103091>.
- Bonnet, S., Reimann, T., Wallinga, J., Lague, D., Davy, P., Lacoste, A., 2019. Landscape dynamics revealed by luminescence signals of feldspars from fluvial terraces. *Sci. Rep.* 9, 8569. <https://doi.org/10.1038/s41598-019-44533-4>.
- Brill, D., Reimann, T., Wallinga, J., May, S.M., Engel, M., Riedesel, S., Brückner, H., 2018. Testing the accuracy of feldspar single grains to date late Holocene cyclone and tsunami deposits. *Quat. Geochronol.* 48, 91–103. <https://doi.org/10.1016/j.quageo.2018.09.001>.
- Del Río, I., Sawakuchi, A.O., González, G., 2019. Luminescence dating of sediments from central Atacama Desert, northern Chile. *Quat. Geochronol.* 53, 101002. <https://doi.org/10.1016/j.quageo.2019.05.001>.
- Diederich, J.L., Wennrich, V., Bao, R., Büttner, C., Bolten, A., Brill, D., Buske, S., Campos, E., Fernández-Galego, E., Gödicke, P., Ninnemann, L., Reyers, M., Ritter, B., Ritterbach, L., Rolf, C., Scheidt, S., Dunai, T.J., Melles, M., 2020. A 68 ka precipitation record from the hyperarid core of the Atacama Desert in northern Chile. *Global Planet. Change* 184, 103054. <https://doi.org/10.1016/j.gloplacha.2019.103054>.
- Dietrich, W.E., Perron, J.T., 2006. The search for a topographic signature of life. *Nature* 439, 411–418. <https://doi.org/10.1038/nature04452>.
- Finch, A.A., Klein, J., 1999. The causes and petrological significance of cathodoluminescence emissions from alkali feldspars. *Contrib. Mineral. Petrol.* 135, 234–243. <https://doi.org/10.1007/s004100050509>.
- Fitzsimmons, K.E., Rhodes, E.J., Barrows, T.T., 2010. OSL dating of southeast Australian quartz: a preliminary assessment of luminescence characteristics and behaviour. *Quaternary Geochronology*, 12th International Conference on Luminescence and Electron Spin Resonance Dating (LED 2008) 5, 91–95. <https://doi.org/10.1016/j.quageo.2009.02.009>.
- Fuchs, M., Owen, L.A., 2008. Luminescence dating of glacial and associated sediments: review, recommendations and future directions. *Boreas* 37, 636–659. <https://doi.org/10.1111/j.1502-3885.2008.00052.x>.
- García-Guinea, J., Townsend, P.D., Sanchez-Muñoz, L., Rojo, J.M., 1999. Ultraviolet-blue ionic luminescence of alkali feldspars from bulk and interfaces. *Phys. Chem. Miner.* 26, 658–667. <https://doi.org/10.1007/s002690050231>.
- Geake, J.E., Walker, G., Mills, A.A., Garlick, G.F.J., 1972. Luminescence of lunar material excited by electrons. *Proceedings of the Lunar Science Conference*, pp. 2971–2977.
- Giardino, J.R., Houser, C., 2015. Principles and dynamics of the critical zone. *Developments in Earth Surface Processes*. Elsevier, Amsterdam Boston.
- Guralnik, B., Jain, M., Herman, F., Ankjærgaard, C., Murray, A.S., Valla, P.G., Preusser, F., King, G.E., Chen, R., Lowick, S.E., Kook, M., Rhodes, E.J., 2015. OSL-thermochronometry of feldspar from the KTB borehole, Germany. *Earth Planet Sci. Lett.* 423, 232–243. <https://doi.org/10.1016/j.epsl.2015.04.032>.
- Huntley, D.J., Baril, M.R., 1997. The K content of the K-feldspars being measured in optical dating or in thermoluminescence dating. *Ancient TL* 15, 3.
- Kars, R.H., Reimann, T., Wallinga, J., 2014. Are feldspar SAR protocols appropriate for post-IR IRSL dating? *Quat. Geochronol.* 22, 126–136. <https://doi.org/10.1016/j.quageo.2014.04.001>.
- Kendall, M.G., Kendall, S.F.H., Smith, B.B., 1939. The distribution of Spearman’s coefficient of rank correlation in a universe in which all rankings occur an equal number of times. *Biometrika* 30, 251–273. <https://doi.org/10.2307/2332649>.
- Kook, M.H., Murray, A.S., Lapp, T., Denby, P.H., Ankjærgaard, C., Thomsen, K., Jain, M., Choi, J.H., Kim, G.H., 2011. A portable luminescence dating instrument. *Nucl. Instrum. Methods Phys. Res. Sect. B Beam Interact. Mater. Atoms* 269, 1370–1378. <https://doi.org/10.1016/j.nimb.2011.03.014>.
- Lambert, R., 2018. Investigating Thermal Decay in K-Feldspar for the Application of IRSL Thermochronometry on the Mont Blanc Massif. *University of Lausanne, Lausanne*.
- Lapp, T., Jain, M., Thomsen, K.J., Murray, A.S., Buylaert, J.-P., 2012. New luminescence measurement facilities in retrospective dosimetry. *Radiat. Meas.* 47, 803–808. <https://doi.org/10.1016/j.radmeas.2012.02.006>.
- Li, B., Jacobs, Z., Roberts, R.G., 2016. Investigation of the applicability of standardised growth curves for OSL dating of quartz from Haaq Fteah cave, Libya. *Quat. Geochronol.* 35, 1–15. <https://doi.org/10.1016/j.quageo.2016.05.001>.
- Li, B., Jacobs, Z., Roberts, R.G., Li, S.-H., 2018. Single-grain dating of potassium-rich feldspar grains: towards a global standardised growth curve for the post-IR IRSL signal. *Quat. Geochronol.* 45, 23–36. <https://doi.org/10.1016/j.quageo.2018.02.001>.

- Li, B., Roberts, R.G., Jacobs, Z., Li, S.-H., 2015a. Potential of establishing a 'global standardised growth curve' (gSGC) for optical dating of quartz from sediments. *Quat. Geochronol.* 27, 94–104. <https://doi.org/10.1016/j.quageo.2015.02.011>.
- Li, B., Roberts, R.G., Jacobs, Z., Li, S.-H., Guo, Y.-J., 2015b. Construction of a 'global standardised growth curve' (gSGC) for infrared stimulated luminescence dating of K-feldspar. *Quat. Geochronol.* 27, 119–130. <https://doi.org/10.1016/j.quageo.2015.02.010>.
- Li, S.-H., Wintle, A.G., 1992. Luminescence sensitivity change due to bleaching of sediments. *International Journal of Radiation Applications and Instrumentation. Part D. Nucl. Tracks Radiat. Meas.* 20, 567–573. [https://doi.org/10.1016/1359-0189\(92\)90006-H](https://doi.org/10.1016/1359-0189(92)90006-H).
- Madsen, A.T., Buylaert, J.-P., Murray, A.S., 2011. Luminescence dating of young coastal deposits from New Zealand using feldspar. *Geochron* 38, 379–390. <https://doi.org/10.2478/s13386-011-0042-5>.
- Mahan, S.A., Rittenour, T.M., Nelson, M.S., Ataei, N., Brown, N., DeWitt, R., Durcan, J., Evans, M., Feathers, J., Frouin, M., Guérin, G., Heydari, M., Huot, S., Jain, M., Keen-Zebert, A., Li, B., López, G.I., Neudorf, C., Porat, N., Rodrigues, K., Sawakuchi, A.O., Spencer, J.Q.G., Thomsen, K., 2022. Guide for interpreting and reporting luminescence dating results. *GSA Bulletin*. <https://doi.org/10.1130/B36404.1>.
- May, S.M., Meine, L., Hoffmeister, D., Brill, D., Medialdea, A., Wennrich, V., Gröbner, M., Schulte, P., Steininger, F., Deprez, M., de Kock, T., Bubbenzer, O., 2020. Origin and timing of past hillslope activity in the hyper-arid core of the Atacama Desert – the formation of fine sediment lobes along the Chuculay Fault System, Northern Chile. *Global Planet. Change* 184, 103057. <https://doi.org/10.1016/j.gloplacha.2019.103057>.
- May, S.M., Zander, A., Francois, J.P., Kelletat, D., Pötsch, S., Rixhon, G., Brückner, H., 2015. Chronological and geoarchaeological investigations on an anthropogenic shell accumulation layer in the Longotoma dune field (Central Chile). *Quat. Int.* 367, 32–41. <https://doi.org/10.1016/j.quaint.2014.06.005>.
- Mueller, D., Preusser, F., 2022. Investigating the applicability of a standardised growth curve approach on Middle Pleistocene sediments from northern Switzerland. *Quat. Geochronol.* 67, 101238. <https://doi.org/10.1016/j.quageo.2021.101238>.
- Murray, A.S., Wintle, A.G., Wallinga, J., 2002. Dose estimation using quartz OSL in the non-linear region of the growth curve. *Radiat. Protect. Dosim.* 101, 371–374. <https://doi.org/10.1093/oxfordjournals.rpd.a006004>.
- Oeser, R.A., Stroncik, N., Moskwa, L.-M., Bernhard, N., Schaller, M., Canessa, R., van den Brink, L., Köster, M., Brucker, E., Stock, S., Fuentes, J.P., Godoy, R., Matus, F.J., Osés Pedraza, R., Osses McIntyre, P., Paulino, L., Seguel, O., Bader, M.Y., Boy, J., Dippold, M.A., Ehlers, T.A., Kühn, P., Kuzyakov, Y., Leinweber, P., Scholten, T., Spielvogel, S., Spohn, M., Übernickel, K., Tielbörger, K., Wagner, D., von Blanckenburg, F., 2018. Chemistry and microbiology of the Critical Zone along a steep climate and vegetation gradient in the Chilean Coastal Cordillera. *Catena* 170, 183–203. <https://doi.org/10.1016/j.catena.2018.06.002>.
- O'Gorman, K., Tanner, D., Sontag-González, M., Li, B., Brink, F., Jones, B.G., Dosseto, A., Jatmiko, Roberts, R.G., Jacobs, Z., 2021. Composite grains from volcanic terranes: internal dose rates of supposed 'potassium-rich' feldspar grains used for optical dating at Liang Bua, Indonesia. *Quat. Geochronol.* 64, 101182. <https://doi.org/10.1016/j.quageo.2021.101182>.
- Peng, J., Li, B., 2017. Single-aliquot Regenerative-Dose (SAR) and Standardised Growth Curve (SGC) Equivalent Dose Determination in a Batch Model Using the R Package 'numOSL' 35.
- Peng, J., Li, B., More, J., Garbow, B., Hillstrom, K., Burkhardt, J., Gilbert, P., Varadhan, R., 2018. numOSL: Numeric Routines for Optically Stimulated Luminescence Dating.
- Prescott, J.R., Fox, P.J., 1993. Three-dimensional thermoluminescence spectra of feldspars. *J. Phys. D Appl. Phys.* 26, 2245–2254. <https://doi.org/10.1088/0022-3727/26/12/024>.
- Reimann, T., Román-Sánchez, A., Vanwallegem, T., Wallinga, J., 2017. Getting a grip on soil reworking – single-grain feldspar luminescence as a novel tool to quantify soil reworking rates. *Quat. Geochronol.* 42, 1–14. <https://doi.org/10.1016/j.quageo.2017.07.002>.
- Reimann, T., Thomsen, K., Jain, M., Murray, A., Frechen, M., 2012. Single-grain dating of young sediments using the pIRIR signal from feldspar. *Quat. Geochronol.* 11, 28–41. <https://doi.org/10.1016/j.quageo.2012.04.016>.
- Reimann, T., Tsukamoto, S., Naumann, M., Frechen, M., 2011. The potential of using K-rich feldspars for optical dating of young coastal sediments – a test case from Darss-Zingst peninsula (southern Baltic Sea coast). *Quat. Geochronol.* 6, 207–222. <https://doi.org/10.1016/j.quageo.2010.10.001>.
- Riedesel, S., Bell, A.M.T., Duller, G.A.T., Finch, A.A., Jain, M., King, G.E., Pearce, N.J., Roberts, H.M., 2021. Exploring sources of variation in thermoluminescence emissions and anomalous fading in alkali feldspars. *Radiat. Meas.* 141, 106541. <https://doi.org/10.1016/j.radmeas.2021.106541>.
- Riedesel, S., King, G.E., Prasad, A.K., Kumar, R., Finch, A.A., Jain, M., 2019. Optical determination of the width of the band-trap states, and the excited and ground state energies of the principal dosimetric tail in feldspar. *Radiat. Meas.* 125, 40–51. <https://doi.org/10.1016/j.radmeas.2018.08.019>.
- Ritter, B., Wennrich, V., Medialdea, A., Brill, D., King, G., Schneiderwind, S., Niemann, K., Fernández-Galego, E., Diederich, J., Rolf, C., Bao, R., Melles, M., Dunai, T.J., 2019. Climatic fluctuations in the hyperarid core of the Atacama Desert during the past 215 ka. *Sci. Rep.* 9, 5270. <https://doi.org/10.1038/s41598-019-41743-8>.
- Román-Sánchez, A., Laguna, A., Reimann, T., Giraldez, J.V., Peña, A., Vanwallegem, T., 2019a. Bioturbation and erosion rates along the soil-hillslope conveyor belt, part 2: quantification using an analytical solution of the diffusion–advection equation. *Earth Surf. Process. Landforms* 44, 2066–2080. <https://doi.org/10.1002/esp.4626>.
- Román-Sánchez, A., Reimann, T., Wallinga, J., Vanwallegem, T., 2019b. Bioturbation and erosion rates along the soil-hillslope conveyor belt, part 1: insights from single-grain feldspar luminescence. *Earth Surf. Process. Landforms* 44, 2051–2065. <https://doi.org/10.1002/esp.4628>.
- Sawakuchi, A.O., Blair, M.W., DeWitt, R., Faleiros, F.M., Hyppolito, T., Guedes, C.C.F., 2011. Thermal history versus sedimentary history: OSL sensitivity of quartz grains extracted from rocks and sediments. *Quat. Geochronol.* 6, 261–272. <https://doi.org/10.1016/j.quageo.2010.11.002>.
- Smedley, R.K., Duller, G.A.T., Pearce, N.J.G., Roberts, H.M., 2012. Determining the K-content of single-grains of feldspar for luminescence dating. *Radiation Measurements. In: Proceedings of the 13th International Conference on Luminescence and Electron Spin Resonance Dating*, 10–14 July, 2011, 47, pp. 790–796. <https://doi.org/10.1016/j.radmeas.2012.01.014>. Toruń, Poland.
- Sontag-González, M., Li, B., O'Gorman, K., Sutikna, T., Jatmiko, Jacobs, Z., Roberts, R.G., 2021. Establishing a pIRIR procedure for De determination of composite mineral grains from volcanic terranes: a case study of sediments from Liang Bua, Indonesia. *Quat. Geochronol.* 65, 101181. <https://doi.org/10.1016/j.quageo.2021.101181>.
- Spearman, C., 1904. The proof and measurement of association between two things. *Am. J. Psychol.* 15, 72–101. <https://doi.org/10.2307/1412159>.
- Spooner, N.A., 1992. Optical dating: preliminary results on the anomalous fading of luminescence from feldspars. *Quaternary Science Reviews, Proceedings of the 6th International Specialist Seminar on Thermoluminescence and Electron Spin Resonance Dating* 11, 139–145. [https://doi.org/10.1016/0277-3791\(92\)90055-D](https://doi.org/10.1016/0277-3791(92)90055-D).
- Starke, J., Ehlers, T.A., Schaller, M., 2020. Latitudinal effect of vegetation on erosion rates identified along western South America. *Science* 367, 1358–1361. <https://doi.org/10.1126/science.aaz0840>.
- Steffen, D., Preusser, F., Schlunegger, F., 2009. OSL quartz age underestimation due to unstable signal components. *Quat. Geochronol.* 4, 353–362. <https://doi.org/10.1016/j.quageo.2009.05.015>.
- Tchakerian, V., Pease, P., 2015. Chapter 14 - the critical zone in desert environments. In: Giardino, J.R., Houser, C. (Eds.), *Developments in Earth Surface Processes*. Elsevier, pp. 449–472. <https://doi.org/10.1016/B978-0-444-63369-9.00014-8>.
- Thomsen, K.J., Murray, A.S., Jain, M., Bøtter-Jensen, L., 2008. Laboratory fading rates of various luminescence signals from feldspar-rich sediment extracts. *Radiat. Meas.* 43, 1474–1486. <https://doi.org/10.1016/j.radmeas.2008.06.002>.
- Tokuyasu, K., Tanaka, K., Tsukamoto, S., Murray, A., 2010. The Characteristics of OSL Signal from Quartz Grains Extracted from Modern Sediments in Japan.
- Veit, H., Preusser, F., Trauerstein, M., 2015. The Southern Westerlies in Central Chile during the two last glacial cycles as documented by coastal aeolian sand deposits and intercalating palaeosols. *Catena* 134, 30–40. <https://doi.org/10.1016/j.catena.2014.11.002>.
- Wei, T., Simko, V., 2023. R Package "Corrplot": Visualization of a Correlation Matrix, Version 0.92.
- Zar, J.H., 2005. Spearman rank correlation. In: Armitage, P., Colton, T. (Eds.), *Encyclopedia of Biostatistics*. Wiley. <https://doi.org/10.1002/0470011815.b2a15150>.
- Zinelabedin, A., Riedesel, S., Reimann, T., Ritter, B., Dunai, T.J., 2022. Testing the potential of using coarse-grain feldspars for post-IR IRSL dating of calcium sulphate-wedge growth in the Atacama Desert. *Quat. Geochronol.* 101341. <https://doi.org/10.1016/j.quageo.2022.101341>.